Infrared conductivity in superconductors with a finite mean free path

N. E. Bickers
Department of Physics, University of Southern California, Los Angeles, California 90089
and Institute for Theoretical Physics, University of California, Santa Barbara, California 93106

D. J. Scalapino
Department of Physics, University of California, Santa Barbara, California 93106

R. T. Collins and Z. Schlesinger
IBM Thomas J. Watson Research Center, Yorktown Heights, New York 10598
(Received 9 August 1989; revised manuscript received 8 January 1990)

We discuss the form of the infrared conductivity and reflectivity in strong-coupling superconductors with a finite mean free path. We restrict attention to the local limit, in which the London penetration depth is much larger than the coherence length. We further assume that the fluctuations responsible for electronic pairing may be treated within a conventional Eliashberg approximation. The conductivity typically exhibits two onsets: one at $2\Delta_0$ and another at $2\Delta_0+\omega_0$, with ω_0 a typical fluctuation energy. The strength of the latter onset relative to the one at $2\Delta_0$ increases as the ratio of the mean free path to the coherence length increases, and in an extremely clean system ($2\Delta_0 \gg \tau^{-1}$) becomes the dominant feature in both the conductivity and reflectivity.

I. INTRODUCTION

Infrared reflectivity measurements, which probe the particle-hole excitation spectrum of a solid, have for many years provided an effective means for studying superconductivity. In the superconducting state, finite-frequency absorption onsets at a frequency $\omega=2\Delta(T)$, where $\Delta(T)$ is the temperature-dependent energy gap. For frequencies below 2Δ, the reflectivity is unity. In dirty metals (i.e., systems with a short mean free path), the reflectivity drops sharply above 2Δ in a manner first calculated by Mattis and Bardeen[1] and by Nam.[2]

Reliable measurements of the gap are of particular interest for the new high-temperature oxide superconductors[3] where the nature of the pairing mechanism and the strength of the coupling are in question. While a number of experimental groups have now obtained data in substantial agreement,[4–11] controversies remain on the interpretation of the data and the possible extraction of an energy gap. We briefly summarize the experimental situation below: for the *a*-*b* plane of $YBa_2Cu_3O_7$ (fully oxygenated), infrared response showing a feature at an unusually large energy scale (700 K $\sim 8T_c$) is seen in the superconducting state.[4] More recent data[8] confirm this and suggest, in addition, the presence of a lower-energy feature. This has been associated with a smaller BCS size gap in the *a*-*b* plane[7] or alternatively with the *c*-axis response.[9] In samples of oxygen-deficient $YBa_2Cu_3O_{7-y}$, evidence for a BCS size gap has also been reported by Thomas *et al.*;[5,10] in the same samples, a second reflectivity feature appears near the large-energy scale observed in fully oxygenated samples. This feature persists to temperatures above 100 K (i.e., significantly above T_c). Finally, it has been suggested[11] that *none* of the infrared features observed so far are associated with the superconducting gap. Kamarás *et al.* argue that in highly stoichiometric crystals the in-plane mean free path may be sufficiently long compared with ξ_0 that the change in reflectivity at $2\Delta_0$ is unobservably small.

The intention of this paper is not to offer a conclusive argument favoring one of the interpretations for infrared measurements mentioned above. A conclusive argument would require quantitative fits for the temperature dependence of spectra above and below T_c in both fully oxygenated and oxygen-deficient samples. In fact, we have found it impossible to obtain a consistent description of spectra *above* T_c, assuming a temperature-independent fluctuation spectrum and constant impurity scattering rate (the assumptions of conventional strong-coupling theory). This is hardly surprising, in view of the anomalous behavior of other properties (e.g., the Cu spin-lattice relaxation rate and the Raman scattering intensity) which cannot be explained within a conventional approach. It might conceivably be possible to obtain a consistent description using a temperature-dependent fluctuation spectrum while retaining the other assumptions of Eliashberg theory. To be meaningful, however, such a spectrum should be calculated explicitly within a model framework or constrained by comparison with other experiments. We have not attempted to address this problem. Instead, we consider here a much more limited problem, namely the dependence of the complex conductivity and reflectivity on the elastic scattering mean free path l in a conventional strong-coupling superconductor. This study addresses in detail the following question: how dirty must a superconductor be to see a clear gap signature in infrared measurements? We expect the answer to be largely independent of the dominant source of scattering (impurity or electron-electron) and the detailed form of the fluctuation spectrum.

Since the early 1960's, the interpretation of energy-gap data and more detailed measurements of excitation spectra has been based on Eliashberg theory.[12] This theory makes a number of assumptions which may be called into question in the new cuprate superconductors. The central assumption, which justifies the neglect of vertex corrections,[13] is that the ratio of the characteristic frequency of the pairing excitations to the Fermi energy is small, i.e., $\omega_0/\epsilon_F \ll 1$. This assumption additionally allows the restriction of calculations to the Fermi surface, reducing $(d+1)$-dimensional integral equations to one-dimensional equations in the frequency variable. This assumption may be violated if pairing in the cuprate systems is mediated by electronic excitations (excitons or magnons), rather than lattice vibrations. In this case, a more detailed calculation, which retains the momentum and frequency dependence of spectra, as well as summing at least a limited class of vertex corrections, is likely to be crucial. In this paper, we assume that such a treatment is not necessary and pursue the effects of a finite mean free path within conventional Eliashberg theory.

Computationally we find it convenient to (i) solve the Eliashberg equations[12] along the Matsubara imaginary frequency axis, (ii) evaluate the conductivity $\sigma(i\omega_m)$ at the Matsubara frequencies $i\omega_m$, and *then* (iii) apply a Padé approximant to analytically continue $\sigma(i\omega_m)$ to the real frequency axis. This procedure, originally[14,15] used to determine H_{c2} and T_c, has proved convenient for evaluating thermodynamic as well as dynamic properties.[16] The remainder of this paper is organized as follows: in Sec. II, we discuss the details of our calculation of the conductivity and reflectivity. In Sec. III, we present and discuss results for mean free paths varying between the clean $(l/\xi_0 \gg 1)$ and dirty $(l/\xi_0 \ll 1)$ limits. Finally, in Sec. IV we summarize our findings and discuss their relevance to the cuprate superconductors.

II. CALCULATION

We assume the applicability of the Migdal-Eliashberg[12,13] approximation for the description of the normal and superconducting states. In this case, the coupling of electrons to fluctuations (phonons or collective electronic excitations) may be described by a single frequency-dependent function α^2F. This function measures the weight in the fluctuation spectrum and the strength of the electron-fluctuation matrix element, appropriately averaged over the Fermi surface. The Nambu matrix Green's function for electrons takes the form

$$G(\mathbf{k},i\omega_n)=(i\omega_n-\epsilon_\mathbf{k}\tau_3-\Sigma_n)^{-1}\;, \tag{2.1}$$

where $\omega_n=(2n+1)\pi T$ is a fermion Matsubara frequency, $\epsilon_\mathbf{k}$ is an eigenvalue of the electronic Hamiltonian, τ_3 is a Pauli matrix, and Σ_n is the self-energy due to scattering from static impurities and fluctuations. The self-energy may be divided into particle-hole diagonal and off-diagonal parts as

$$\Sigma_n=(1-Z_n)i\omega_n+\phi_n\tau_1\;. \tag{2.2}$$

Here Z_n is the mass renormalization function, and $\phi_n=Z_n\Delta_n$ is the renormalized gap function. The Green's function may be rewritten as

$$\begin{aligned}G(\mathbf{k},i\omega_n)&=(i\omega_nZ_n-\epsilon_\mathbf{k}\tau_3-\phi_n\tau_1)^{-1}\\&=-\frac{i\omega_nZ_n+\epsilon_\mathbf{k}\tau_3+\phi_n\tau_1}{(Z_n\omega_n)^2+\epsilon_\mathbf{k}^2+\phi_n^2}\;.\end{aligned} \tag{2.3}$$

This form is valid for both the superconducting state and the normal state, where $\phi_n=0$.

Assuming particle-hole symmetry, the functions Z_n and ϕ_n are real, and

$$\begin{aligned}Z_{-n}&=Z_n\;,\\\phi_{-n}&=\phi_n\;.\end{aligned} \tag{2.4}$$

In the Eliashberg approximation, the contributions to Σ from interaction with impurities and fluctuations take the diagrammatic form shown in Fig. 1. The double lines indicate that the electron Green's functions must be determined self-consistently. After carrying out the momentum sums implied by the diagrams, the self-energy reduces to

$$\begin{aligned}\omega_n(1-Z_n)&=-\frac{1}{2\tau}\frac{\omega_nZ_n}{[(Z_n\omega_n)^2+\phi_n^2]^{1/2}}\\&\quad-\pi T\sum_m\lambda_{n-m}\frac{\omega_mZ_m}{[(Z_m\omega_m)^2+\phi_m^2]^{1/2}}\;,\\\phi_n&=\frac{1}{2\tau}\frac{\phi_n}{[(Z_n\omega_n)^2+\phi_n^2]^{1/2}}\\&\quad+\pi T\sum_m\lambda_{n-m}\frac{\phi_m}{[(Z_m\omega_m)^2+\phi_m^2]^{1/2}}\;.\end{aligned} \tag{2.5}$$

Here τ^{-1} is the impurity scattering rate, and

$$\lambda_{n-m}=\int_0^\infty d\omega\,\alpha^2F(\omega)\frac{2\omega}{\omega^2+(\omega_n-\omega_m)^2}\;. \tag{2.6}$$

Thus, the self-energy follows from solution of two coupled matrix equations in the single variable ω_n.

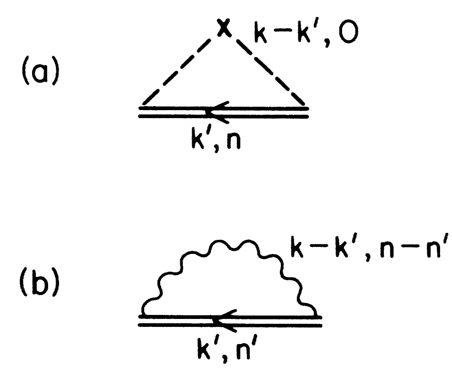

FIG. 1. Contributions to the electronic self-energy Σ. The self-consistent Nambu Green's function is indicated by a double line. (a) Static impurity scattering. (b) Dynamic fluctuation scattering.

After solving for the Green's function, it is necessary to evaluate the current-current correlation function[2] to find the conductivity. One could imagine using a Padé approximant to continue (Z_n,ϕ_n) to $(Z(\omega),\phi(\omega))$ and then calculating $\sigma(\omega)$ as a real-frequency integral involving $Z(\omega)$ and $\phi(\omega)$. However, we believe that, having found Z_n and ϕ_n, it is better to proceed by evaluating the current-current correlation function $\Pi(i\nu_m)$ within the Matsubara formalism. After this is done, a Padé approximant[16] may be used to carry out the analytic continuation directly on the physical quantity of interest. Thus, we have

$$\sigma(\omega)=\frac{i\Pi(i\nu_m\to\omega+i0^+)}{\omega}\ , \tag{2.7}$$

with

$$\Pi(i\nu_m)=\frac{2T}{N}\sum_{n\mathbf{k}}\mathrm{Tr}\frac{ek_x}{m}G(\mathbf{k},i(\omega_n+\nu_m))G(\mathbf{k},i\omega_n)\Gamma_x\ . \tag{2.8}$$

This correlation function is represented diagrammatically in Fig. 2. Note that $\nu_m=2m\pi T$ is a boson Matsubara frequency. The factor of 2 follows from a sum over spins, and the trace is taken over particle-hole degrees of freedom. The momentum transfer $\mathbf{q}$ has been set to 0, as is appropriate in the local limit ($\xi_0\ll\lambda$).

To lowest order, the vertex Γ_x is just ek_x/m; however, in order to be consistent with the Eliashberg approximation used to evaluate single-particle self-energies, the vertex should properly include a ladder summation of impurity and fluctuation scattering processes. For isotropic impurity scattering, the effect of such corrections is to replace the quasiparticle lifetime τ with a transport time τ_{tr}. The transport time is longer than the lifetime, since forward scattering events (i.e., those with small momentum transfer) are ineffective in reducing the current. *Qualitatively,* the effect of vertex corrections for dynamic scattering is expected to be similar: the coupling function α^2F should be replaced by a transport function $\alpha^2_{\mathrm{tr}}F$, which incorporates a reduced matrix element for small-momentum-transfer processes before calculating Fermi surface averages. We do not attempt to address this complication, but instead *assume* the replacement $\alpha^2F\to\alpha^2_{\mathrm{tr}}F$ is sufficient. Note that this phenomenological treatment of vertex corrections prevents a rigorous simultaneous calculation of the conductivity and static properties, such as T_c. This is because the relationship between α^2F and $\alpha^2_{\mathrm{tr}}F$ can only be established by an *ab initio* calculation based on a Fermi surface, fluctuation spectrum, and matrix elements; neglecting the differences in these spectra amounts to neglecting vertex corrections entirely.

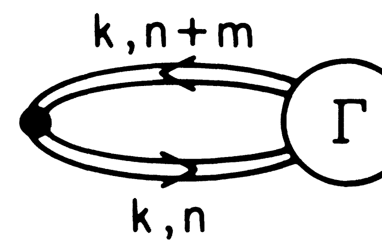

FIG. 2. Current-current correlation function $\Pi(i\nu_m)$. The solid dot represents the lowest-order vertex $v_x=ek_x/m$. Only a single complete vertex Γ_x appears, to prevent double counting.

As usual, the momentum summation in Eq. (2.8) may be reduced to a Fermi surface average and an energy integration. The Fermi surface average gives

$$2e^2N(0)\langle v_x^2\rangle\simeq ne^2/m=\omega_P^2/4\pi\ , \tag{2.9}$$

with n the electronic density and ω_P the plasma frequency. This identification rigorously holds for a spherical Fermi surface. The energy integration gives

$$\begin{aligned}
&\int d\epsilon_k\mathrm{Tr}G(\mathbf{k},i(\omega_n+\nu_m))G(\mathbf{k},i\omega_n)=\pi S_{nm}\ ,\\
S_{nm}&=\frac{\tilde\omega_n(\tilde\omega_n+\tilde\omega_{n+m})+\phi_n(\phi_n-\phi_{n+m})}{R_nP_{nm}}-\frac{\tilde\omega_{n+m}(\tilde\omega_{n+m}+\tilde\omega_n)+\phi_{n+m}(\phi_{n+m}-\phi_n)}{R_{n+m}P_{nm}}\quad(m\neq0,-2n-1)\\
&=\frac{\phi_n^2}{R_n^3}\quad(m=0)\\
&=\frac{1}{R_n}\quad(m=-2n-1)\ ,
\end{aligned} \tag{2.10}$$

where

$$\begin{aligned}
\tilde\omega_n&=Z_n\omega_n\ ,\\
R_n&=(\tilde\omega_n^2+\phi_n^2)^{1/2}\ ,\\
P_{nm}&=\tilde\omega_n^2-\tilde\omega_{n+m}^2+\phi_n^2-\phi_{n+m}^2\ .
\end{aligned} \tag{2.11}$$

Thus, the current-current correlation function reduces to

$$\Pi(i\nu_m)=\frac{\omega_P^2}{4\pi}\pi T\sum_n S_{nm}\ . \tag{2.12}$$

The conductivity must still be calculated by an analytic continuation to the real axis. It is convenient to separate the imaginary-axis conductivity into separate contributions from the superconducting condensate and additional excitations:

$$\sigma(i\nu_m)=\sigma_{sc}(i\nu_m)+\sigma_{exc}(i\nu_m) ,$$
$$\sigma_{sc}(i\nu_m)=i\frac{\Pi(0)}{i\nu_m} , \quad (2.13)$$
$$\sigma_{exc}(i\nu_m)=i\frac{\Pi(i\nu_m)-\Pi(0)}{i\nu_m} .$$

Note from Eq. (2.10) that σ_{sc} vanishes identically in the normal state. The analytic continuation of σ_{sc} is just

$$\sigma_{sc}(\omega)=\pi\Pi(0)\delta(\omega)+i\frac{\Pi(0)}{\omega} . \quad (2.14)$$

The analytic continuation of σ_{exc} is nonsingular. We have employed the Padé approximant technique of Vidberg and Serene[16] to perform this continuation numerically. The accuracy of the continuation may be checked by a number of means, including the conductivity sum rule,[17] which states that the integrated weight in the real part of the conductivity σ_1 must be the same in the superconducting state and in a hypothetical normal state at the same temperature:

$$\int_{-\infty}^{\infty} d\omega\, \sigma_{1S}(\omega)=\int_{-\infty}^{\infty} d\omega\, \sigma_{1N}(\omega) . \quad (2.15)$$

This sum rule simply indicates that the weight removed from the spectrum at low energies in the superconducting state must reappear in the δ function at zero frequency.

Finally, the real-frequency conductivity may be used to calculate the reflectivity measured experimentally. For normal incidence, the reflectivity takes the general form

$$R=\left|\frac{\sqrt{\epsilon}-1}{\sqrt{\epsilon}+1}\right|^2 , \quad (2.16)$$

with ϵ the frequency-dependent complex dielectric function. For a system in which the response of the background ions may be modeled entirely by a constant contribution ϵ_∞, the dielectric constant may be written

$$\epsilon(\omega)=\epsilon_\infty+\frac{4\pi i\sigma}{\omega} . \quad (2.17)$$

For simplicity, we have assumed $\epsilon_\infty=1$ in our calculations.

III. RESULTS AND DISCUSSION

To illustrate the effects of a finite mean free path on the conductivity and reflectivity, we show below results for a model fluctuation spectrum with impurity scattering which varies from the clean to dirty limit. In each case, we assume the electrodynamics remains local in the superconducting state, i.e., that $\xi_0 \ll \lambda$. (This is thought to be the situation in all the high-temperature cuprate materials.)

For simplicity, the fluctuation spectrum is assumed to be a single truncated Lorentzian with peak position ω_0, width Γ_0, and truncation width Γ_c:

$$F(\omega)=A\left[\frac{1}{(\omega-\omega_0)^2+\Gamma_0^2}-\frac{1}{\Gamma_c^2+\Gamma_0^2}\right] \quad |\omega-\omega_0|<\Gamma_c$$
$$=0 \quad |\omega-\omega_0|>\Gamma_c , \quad (3.1)$$

TABLE I. Ratio of the mean free path and zero-temperature coherence length $l/\xi_0=\pi\Delta_0(\hbar/\tau)^{-1}$ for the scattering rates $\hbar/\tau$ assumed in Figs. 5–9.

$\hbar/\tau$	l/ξ_0
0	∞
5 meV	8
50 meV	0.8
500 meV	0.08

with A chosen to normalize the spectrum to unity. With this convention, the coupling constant α_{tr}^2 has units of energy.

For the plots shown here, we have chosen the following set of generic parameters: $\omega_0=50$ meV, $\Gamma_0=5$ meV, $\Gamma_c=3\Gamma_0=15$ meV, and $\alpha^2=25$ meV. We have assumed impurity scattering rates $\hbar/\tau$ of 0, 5, 50, and 500 meV. Finally, we have arbitrarily chosen a plasma frequency ω_P of 1 eV. With these parameters, the pure-metal coupling strength λ, defined by the relation

$$Z(0)=1+\lambda , \quad (3.2)$$

is 0.94. The zero-temperature superconducting energy gap is defined by the relation

$$\mathrm{Re}\Delta(\Delta_0)=\Delta_0 . \quad (3.3)$$

This value is independent of impurity scattering and is calculated to be 12.1 meV. The associated value of $2\Delta_0/kT_c$ is 4.2. A dimensionless measure of the strength of impurity scattering is the ratio l/ξ_0. Assuming $l=v_F\tau$ and $\xi_0=\hbar v_F/\pi\Delta_0$ gives $l/\xi_0=\pi\Delta_0(\hbar/\tau)^{-1}$.[18] The ratios l/ξ_0 for each assumed value of $\hbar/\tau$ are given in Table I.

In Figs. 3 and 4, we display the frequency-dependent renormalization function Z and gap function Δ which follow from the solution of the Eliashberg equations for

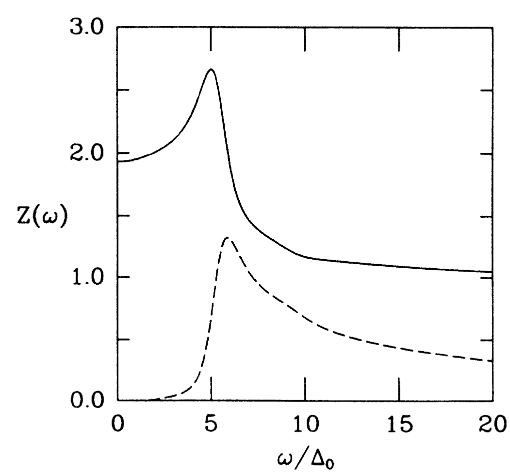

FIG. 3. Frequency-dependent renormalization function $Z(\omega)$ in the superconducting state. The impurity scattering rate is 0. Parameters for the fluctuation spectrum are given in the text. The solid line indicates the real part Z_1 and the dashed line the imaginary part Z_2.

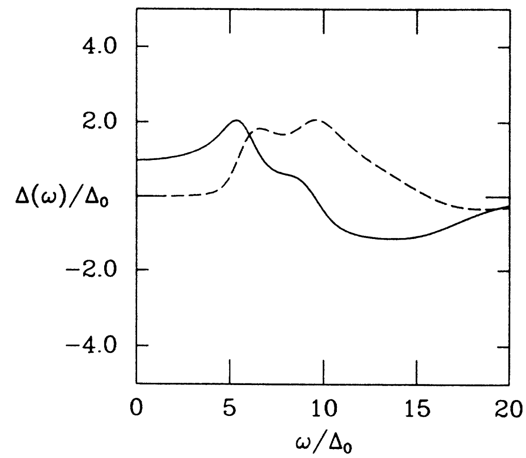

Fig. 4. Frequency-dependent gap function $\Delta(\omega)$. Parameters are as in Fig. 3. The solid line indicates the real part Δ_1 and the dashed line the imaginary part Δ_2.

$\tau^{-1}=0$. These functions have been calculated on the real axis using the Padé approximant technique of Vidberg and Serene[16] to analytically continue imaginary-axis data. The imaginary-axis calculation was carried out at a temperature of 1 meV (effectively the zero-temperature limit) using 200 positive Matsubara frequencies, a number sufficient to insure convergence. The continuation was performed using 190 frequencies.

Both Z and Δ are plotted as functions of ω/Δ_0. The peak in the fluctuation spectrum occurs at $\omega_0/\Delta_0=4.1$. The real part of the renormalization function Z_1 is $1+\lambda$ at low frequencies, passes through a maximum near $\Delta_0+\omega_0$, and decays rapidly to unity at higher energies. The imaginary part of the renormalization function Z_2 is strictly zero below Δ_0 , the lowest allowed quasiparticle energy; a peak occurs at $\Delta_0+\omega_0$, where single-phonon emission is resonant. A weaker shoulder reflecting two-phonon emission occurs near $\Delta_0+2\omega_0$. The real part of the gap function Δ_1 reflects the sign of the frequency-dependent electron-electron interaction induced by ex-

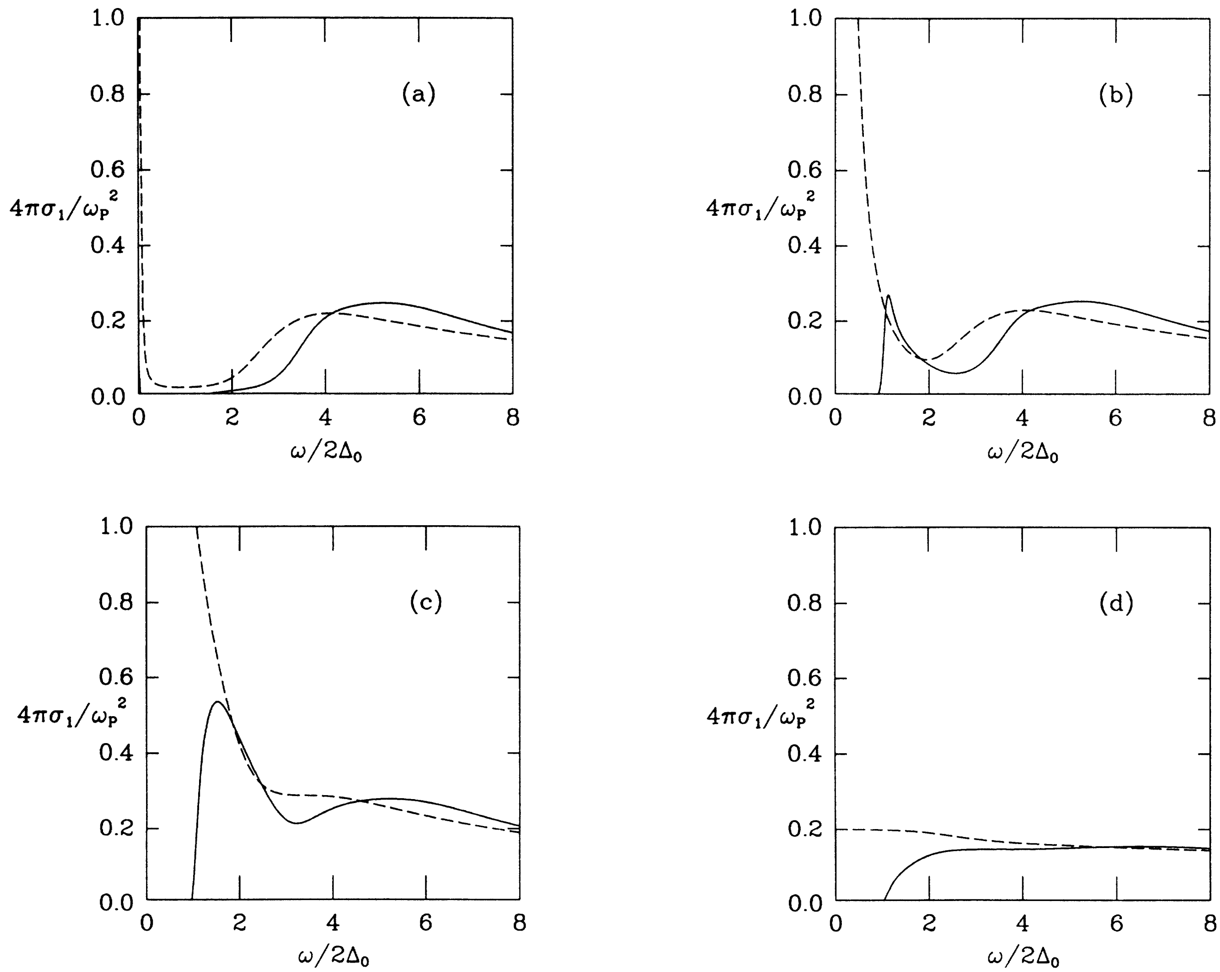

FIG. 5. Real part of the conductivity σ_1 for various impurity scattering rates $\hbar/\tau$. In each plot, a solid line indicates the superconducting-state conductivity σ_{1S} and a dashed line the normal-state conductivity σ_{1N}. The scattering rates are (a) 0, (b) 5 meV, (c) 50 meV, and (d) 500 meV.

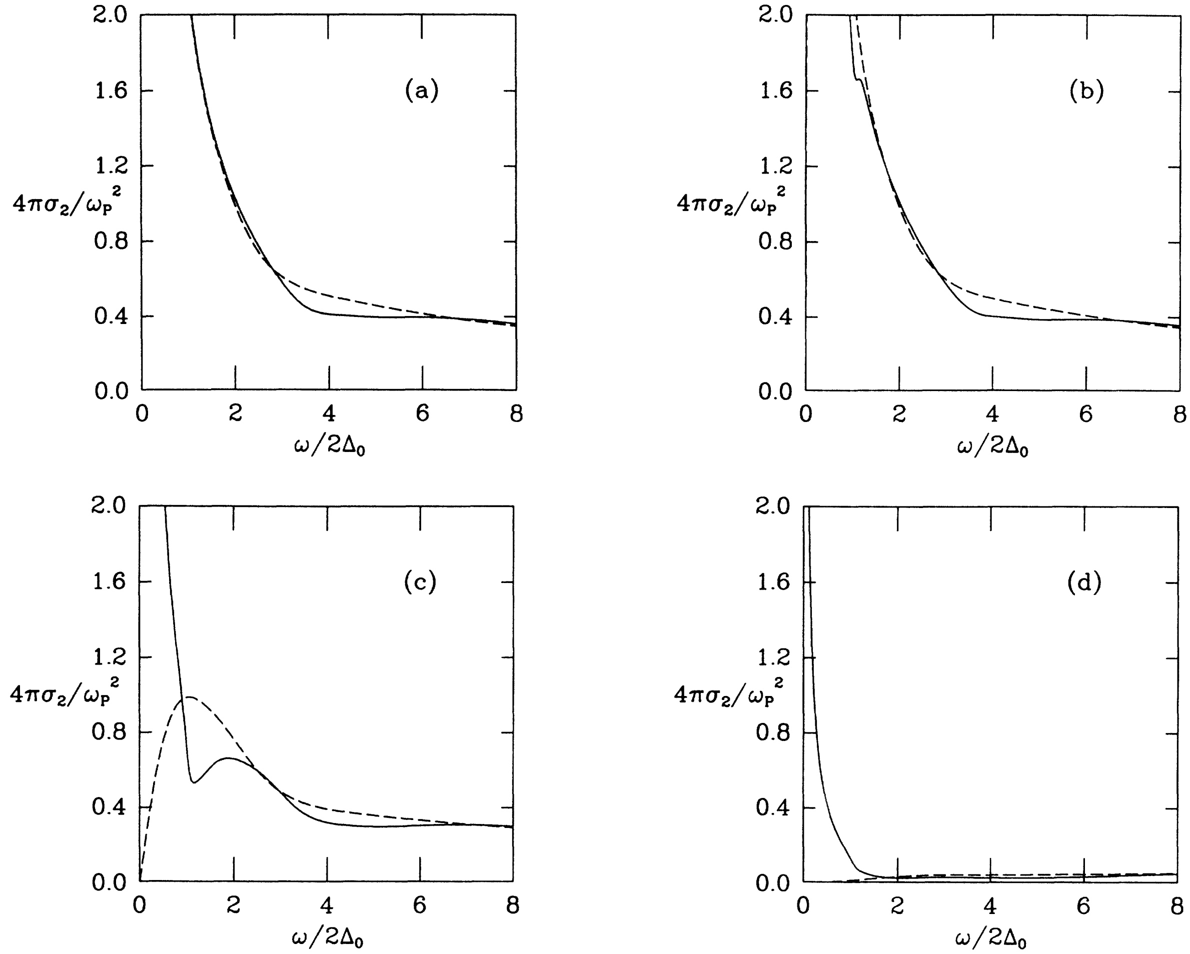

FIG. 6. Imaginary part of the conductivity σ_2 for various impurity scattering rates. As in Fig. 5, a solid line indicates the superconducting-state conductivity, and a dashed line the normal-state conductivity. The scattering rates are (a) 0, (b) 5 meV, (c) 50 meV, and (d) 500 meV.

change of fluctuations: it is positive at low frequencies, where the interaction is attractive; passes through a maximum near $\Delta_0+\omega_0$, where the interaction is resonant; and becomes negative at high frequencies, where the interaction is repulsive. Like Z_2, the imaginary part of the gap Δ_2 is strictly zero below Δ_0 and exhibits peaks near $\Delta_0+\omega_0$ and $\Delta_0+2\omega_0$.

For each choice of the impurity scattering rate, a normal-state and superconducting-state conductivity have been calculated using the method described in Sec. II. In each case, the conductivity sum rule holds to better than 1% accuracy. Results for the real (σ_1) and imaginary (σ_2) parts of the conductivity are shown in Figs. 5 and 6. Note that the frequency is measured in units of $2\Delta_0$, and that in these units the fluctuation frequency ω_0 is 2.1. (Calculations of the normal-state conductivity at this same temperature, 1 meV, assume $\phi_n\equiv 0$. Neglecting normal-state magnetoresistance, this condition would be achieved in a hypothetical experiment by applying a magnetic field larger than H_{c2}.) The frequency-dependent ratio σ_{1S}/σ_{1N} is plotted in Fig. 7.

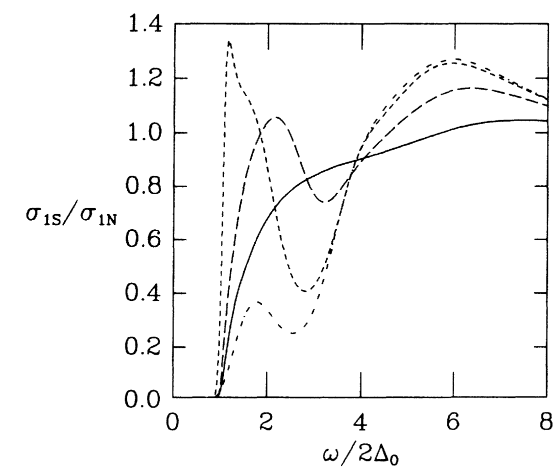

FIG. 7. Superconducting-to-normal-state conductivity ratio, σ_{1S}/σ_{1N}. The impurity scattering rates are 0 (dash-dotted line), 5 meV (short-dashed line), 50 meV (long-dashed line), and 500 meV (solid line).

For a pure system [Figs. 5(a) and 6(a)], the normal-state conductivity is particularly simple: in the zero-temperature limit, σ_{1N} diverges at $\omega=0$ and vanishes at finite frequencies below the threshold for creation of real fluctuations, near ω_0. (The electronic system has essentially the behavior of a pure electron gas below this frequency.) In the superconducting state, the conductivity vanishes below the pair-breaking threshold at $2\Delta_0$, and in the region between $2\Delta_0$ and $2\Delta_0+\omega_0$, the conductivity remains extremely small. This additional gap in the absorption spectrum has the same origin as that in the normal state: In the absence of impurities and dynamic fluctuations, a photon in this energy range cannot be converted to a particle-hole pair with conservation of both energy and momentum. The feature distinguishing σ_{1S} from σ_{1N} is the *shift* in the threshold for creation of fluctuations by $2\Delta_0$. Thus, in the clean limit, the gap can, in principle, be measured indirectly by detecting this shift, but not by directly observing where σ_{1S} rises from zero.

In a system with weak impurity scattering [Figs. 5(b) and 6(b)], the normal-state conductivity is a superposition of Drude and fluctuation terms. As before, the fluctuation contribution onsets near ω_0. The width of the Drude contribution is proportional to the scattering rate. In the superconducting state, the threshold for scattering with creation of fluctuations is again shifted to $2\Delta_0+\omega_0$. However, in this case, the presence of impurities allows photon absorption arbitrarily close to the particle-hole threshold at $2\Delta_0$. The detailed variation of σ_{1S} near the threshold is determined by a competition between the decreasing rate for impurity-assisted absorption and the increasing phase space provided by the frequency-dependent coherence factors in the superconducting state.[19] The energy scale for variations in the impurity-assisted absorption rate is $\hbar/\tau$ and the scale for variations in the coherence factors is $2\Delta_0$. In general, one expects a peak in σ_{1S} near $2\Delta_0$ when these scales are comparable, or alternatively when $l/\xi_0\sim 1$. So long as $\hbar/\tau$ is smaller than or of order ω_0, this peak should be distinguishable from the onset of absorption with creation of fluctuations at $2\Delta_0+\omega_0$. This behavior is clearly exhibited in Fig. 5(b). As in Fig. 5(a), the gross difference between σ_{1S} and σ_{1N} is an overall shift in the superconducting spectrum by $2\Delta_0$. So long as the peak in σ_{1S} at $2\Delta_0$ is distinguishable above the background, the gap may now be read off directly from σ_{1S}. However, as discussed below, while the peak at $2\Delta_0$ appears clearly in $\sigma_1(\omega)$ it is much more difficult to see in the reflectivity.

When the impurity scattering is further increased so that $l\simeq\xi_0$, the qualitative features of the conductivity [Figs. 5(c) and 6(c)] remain as above. As expected, the clear separation of Drude and fluctuation contributions begins to disappear as $\hbar/\tau$ becomes comparable to ω_0.

Finally, when the impurity scattering becomes very strong [$l/\xi_0=0.08$ in Figs. 5(d) and 6(d)], the conductivity assumes the classic form for a dirty superconductor. The normal-state conductivity σ_{1N} is, in this case, dominated by the Drude contribution and is nearly constant on the scale of $2\Delta_0$. This fact simplifies the behavior in the superconducting state: since scattering is strong and nearly frequency independent just above the threshold $2\Delta_0$, the variation of σ_{1S} is controlled by the density of states and the coherence factors. This should be contrasted with behavior in the clean limit [Figs. 5(b) and 6(b)].

The ratio σ_{1S}/σ_{1N}, shown in Fig. 7, assumes a simple form only in the dirty limit $l/\xi_0\ll 1$. In the clean limit $l/\xi_0\gg 1$, the ratio is complicated by the appearance of two distinct contributions to σ_1 in *both* the normal and superconducting states and the relative displacement of the spectra by $2\Delta_0$. In contrast, in the dirty limit, the ratio assumes the strong-coupling form first obtained by Nam:[2] the normal-state conductivity is essentially constant, and variations in the ratio are controlled by the energy-dependent coherence factors in the superconducting state. The result for σ_{1S}/σ_{1N} is a slight modification of the universal curve obtained by Mattis and Bardeen[1] for dirty weak-coupling superconductors: as shown in Fig. 7, the only effect is a mild depression in the ratio near $2\Delta_0+\omega_0$ and a comparable enhancement at high energies (both reflecting the shift in the fluctuation emission threshold).

Experiments in the infrared generally measure the reflectivity $R(\omega)$. Although the conductivity may be extracted by performing a Kramers-Kronig analysis or making various model fits to the data, it is interesting to use the theoretical results for σ to calculate R directly from Eq. (2.16). In Fig. 8, results for R in the normal and superconducting states are plotted for the impurity scattering rates discussed above. The ratio of superconducting- and normal-state reflectivities R_S/R_N is plotted in Fig. 9.

In the clean limit [$\hbar/\tau=0$ in Fig. 8(a)], the normal-state reflectivity R_N remains close to unity for frequencies up to ω_0, the fluctuation emission threshold. In the intermediate regime, where τ^{-1} is roughly comparable to $2\Delta_0$ and ω_0 (shown by the long-dashed curve in Fig. 8), two clear breaks are observed in R_N, corresponding to the onset of absorption with impurity scattering at zero frequency and the onset of absorption with fluctuation emission at ω_0. In the dirty limit ($\hbar/\tau=500$ meV in the figure), R_N assumes a conventional Drude form, and the effects of finite-frequency fluctuations are masked by the large impurity contribution.

Each superconducting reflectivity R_S [Fig. 8(b)] closely resembles the corresponding R_N with an overall shift by $2\Delta_0$. As in the case of the conductivity, the energy gap $2\Delta_0$ is obscured in the extreme clean limit by the absence of strong low-frequency scattering. Only for values of $l/\xi_0\leq 1$ is a large drop in R_S observed at the gap energy. In both the intermediate regime ($l/\xi_0\simeq 1$) and the dirty limit $l/\xi_0\ll 1$), a drop in R_S is observed at the gap energy. In the clean limit, the drop in R_S occurs at $2\Delta_0+\omega_0$.

Finally, the ratio R_S/R_N is plotted in Fig. 9. This ratio shows two characteristic features, a gap at $2\Delta_0$ and a Holstein step at $2\Delta_0+\omega_0$. We note that the gap feature at $2\Delta_0$ is absent for $\tau^{-1}=0$ and grows relative to the Holstein step as τ^{-1} is increased. The magnitude of the gap feature relative to the Holstein step scales roughly as ξ_0/l.

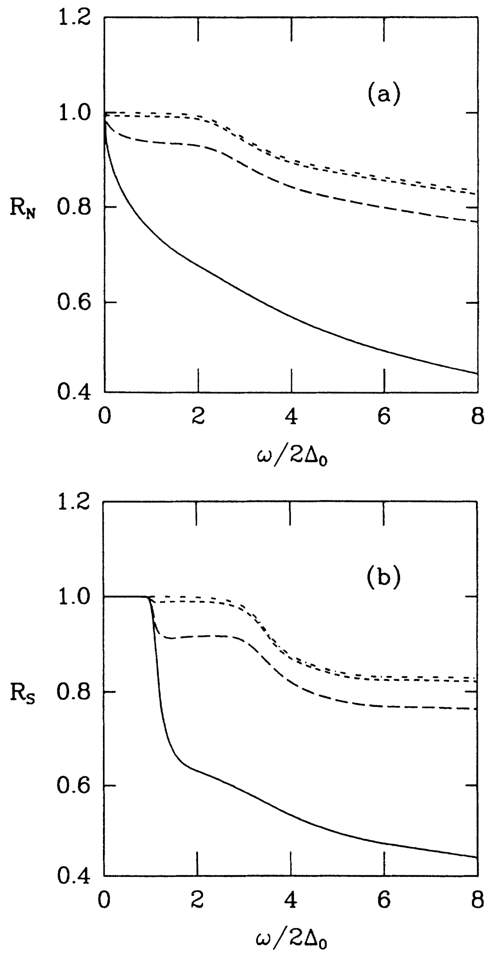

FIG. 8. Reflectivity in the normal (a) and superconducting (b) states. The impurity scattering rates are 0 (dash-dotted line), 5 meV (short-dashed line), 50 meV (long-dashed line), and 500 meV (solid line).

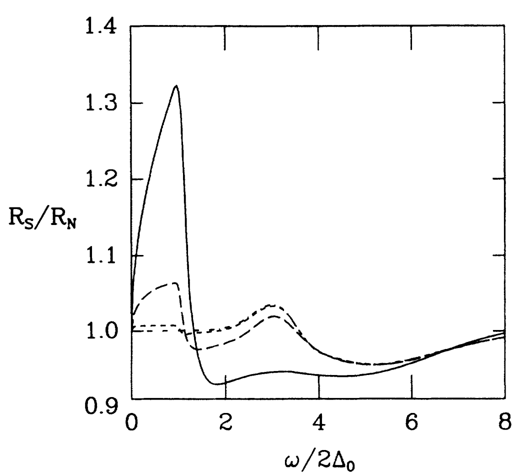

FIG. 9. Superconducting-to-normal-state reflectivity ratio, R_S/R_N. The impurity scattering rates are 0 (dash-dotted line), 5 meV (short-dashed line), 50 meV (long-dashed line), and 500 meV (solid line).

IV. CONCLUSIONS

The short coherence length of the recently discovered high-temperature cuprate superconductors implies that they obey a local electrodynamics, even in the clean limit. In these systems, ξ_0 is thought to be of order 10–30 Å. Estimates of the mean free path at T_c in $YBa_2Cu_3O_{7-y}$ range from tens to hundreds of angstroms. Within the conventional model investigated above, the precise value of l/ξ_0 determines whether the system falls in the intermediate regime ($l/\xi_0 \sim 1$) or the extreme clean limit ($l/\xi_0 \gg 1$). (In $YBa_2Cu_3O_{7-y}$, the mean free path is strongly temperature dependent, and the value of l at the transition temperature should be used in determining this ratio.) In the intermediate regime, both the gap $2\Delta_0$ and the Holstein feature at $2\Delta_0+\omega_0$ should be observable; however, in the extreme clean limit, as we have seen in Sec. III, it becomes difficult to determine $2\Delta_0$ experimentally. As shown in Fig. 8, a change in reflectivity at approximately the 1% level is expected at $\omega=2\Delta_0$ even for $l/\xi_0 \sim 10$. Based on this line of reasoning, the gap in $YBa_2Cu_3O_{7-y}$ should be barely visible in infrared measurements, i.e., the system should be dirty enough to measure $2\Delta_0$.

As emphasized in Sec. I, the interpretation of experimental reflectivity data for $YBa_2Cu_3O_{7-y}$ remains controversial. Furthermore, the present Migdal-Eliashberg study, based on a temperature-independent fluctuation spectrum and constant impurity scattering rate, is not sufficiently general to argue conclusively in favor of a particular experimental interpretation. Nevertheless, it is possible to point out qualitative features which follow from applying the Migdal-Eliashberg analysis to the interpretations of Thomas *et al.*[5] and of Schlesinger *et al.*[4] We do not describe here the arguments for and against these interpretations.[4–11]

A change in reflectivity of order 1% was detected by Thomas *et al.*[5] in oxygen-deficient samples of $YBa_2Cu_3O_{7-y}$ at a frequency consistent with BCS-like behavior. As argued above, a reflectivity change of this size seems consistent with estimates of l/ξ_0 in this system. Within the simple Migdal-Eliashberg picture, the higher-energy excitation detected in the Thomas *et al.* study would correspond to the fluctuation peak (or Holstein feature) at $2\Delta_0+\omega_0$; indeed a conductivity spectrum resembling Fig. 5(b) has been obtained experimentally.[10] Since the peak in the fluctuation spectrum may itself be temperature dependent [i.e., $\omega_0=\omega_0(T)$], we hesitate to draw additional conclusions based on the temperature dependence of this feature. The high-energy feature in fully oxygenated samples would also necessarily be identified as a fluctuation peak within this scenario.

Within the alternate scenario of Schlesinger *et al.*,[4] a drop in reflectivity at $\omega \sim 700$ K$=8T_c$ in fully oxygenated samples is interpreted as the superconducting gap. The reflectivity and conductivity spectra above this energy are relatively featureless, providing no evidence for a fluctuation peak of the type expected within a Migdal-Eliashberg analysis. A fluctuation peak might not be detected if (a) ω_0 is anomalously large, i.e., the coupling is actually "weak" and the large $2\Delta_0/kT_c$ ratio is due to unrelated pair-breaking processes near T_c, or (b) the relevant fluctuation spectrum is broad, featureless, and temperature dependent.

In summary, our main conclusion with regard to $YBa_2Cu_3O_{7-y}$ is that the infrared gap should be visible, i.e., the scattering rate is not small enough to make the gap undetectable. While the Migdal-Eliashberg picture can be applied qualitatively to several conflicting interpretations of the experimental data, the present assumptions are not sufficiently general for a quantitative analysis, i.e., fits for the full temperature dependence of spectra in both oxygenated and oxygen-deficient samples.

ACKNOWLEDGMENTS

We wish to thank A. J. Millis and J. Orenstein for useful discussions. This research was supported in part by the National Science Foundation under Grants Nos. DMR86-15454, DMR89-13850, and PHY82-17853, supplemented by funds from the National Aeronautics and Space Administration.

---

[1]D. C. Mattis and J. Bardeen, Phys. Rev. **111**, 412 (1958).

[2]S. B. Nam, Phys. Rev. **156**, 470 (1967); **156**, 487 (1967).

[3]J. G. Bednorz and K. A. Müller, Z. Phys. B **64**, 18 (1986); M. K. Wu, J. R. Ashburn, C. J. Torng, P. H. Hor, R. L. Meng, L. Gao, Z. J. Huang, X. Q. Wang, and C. W. Chu, Phys. Rev. Lett. **58**, 908 (1987).

[4]Z. Schlesinger, R. T. Collins, D. L. Kaiser, and F. Holtzberg, Phys. Rev. Lett. **59**, 1938 (1987).

[5]G. A. Thomas, J. Orenstein, D. H. Rapkine, M. Capizzi, A. J. Millis, L. F. Schneemeyer, and J. V. Waszczak, Phys. Rev. Lett. **61**, 1313 (1988).

[6]T. Timusk, S. L. Herr, K. Kamarás, C. D. Porter, D. B. Tanner, D. A. Bonn, J. D. Garrett, C. V. Stager, J. E. Greedan, and M. Reedyk, Phys. Rev. B **38**, 6683 (1988).

[7]J. Schützmann, W. Ose, J. Keller, K. F. Renk, B. Roas, L. Schultz, and G. Saemann-Ischenko, Europhys. Lett. **8**, 679 (1989).

[8]T. Timusk and D. B. Tanner, in *Physical Properties of High Temperature Superconductors I,* edited by D. M. Ginsberg (World-Scientific, Singapore, 1989), p. 339.

[9]R. T. Collins, Z. Schlesinger, F. Holtzberg, and C. Feild, Phys. Rev. Lett. **63**, 422 (1989).

[10]J. Orenstein, G. A. Thomas, A. J. Millis, S. L. Cooper, D. H. Rapkine, T. Timusk, L. F. Schneemeyer, and J. V. Waszczak, Phys. Rev. B (to be published).

[11]K. Kamarás, S. L. Herr, C. D. Porter, N. Tache, D. B. Tanner, S. Etemad, T. Venkatesan, E. Chase, A. Inam, X. D. Wu, M. S. Hegde, and B. Dutta, Phys. Rev. Lett. **64**, 84 (1990).

[12]G. M. Eliashberg, Zh. Eksp. Teor. Fiz. **38**, 966 (1960) [Sov. Phys.—JETP **11**, 696 (1960)].

[13]A. B. Migdal, Zh. Eksp. Teor. Fiz. **34**, 1438 (1958) [Sov. Phys.—JETP **7**, 996 (1958)].

[14]E. D. Yorke and A. Bardasis, Phys. Rev. **159**, 344 (1967).

[15]C. S. Owen and D. J. Scalapino, Physica **55**, 691 (1971).

[16]H. J. Vidberg and J. Serene, J. Low. Temp. Phys. **29**, 179 (1977).

[17]R. A. Ferrell and R. E. Glover, Phys. Rev. **109**, 1398 (1958); M. Tinkham and R. A. Ferrell, Phys. Rev. Lett. **2**, 331 (1959).

[18]In the presence of low-energy fluctuations, the width of the Drude peak measured in infrared experiments is not $1/\tau$, but $1/\tau^*$, with $\tau^*=(1+\lambda)\tau$. This renormalization must be taken into account in extracting an experimental estimate of l/ξ_0 for comparison with the theory.

[19]Similar results, showing the effect of l/ξ_0 on the onset of absorption at $2\Delta_0$, for the weak-coupling BCS theory, have been reported by J. J. Chang and D. J. Scalapino, Phys. Rev. B **40**, 4299 (1990).